A multi-scale atomistic-continuum modelling of crack propagation in a two-dimensional macroscopic plate

1998 J. Phys.: Condens. Matter 10 2375

(http://iopscience.iop.org/0953-8984/10/11/003)

J. Phys.: Condens. Matter **10** (1998) 2375–2387. Printed in the UK PII: S0953-8984(98)84930-8

A multi-scale atomistic-continuum modelling of crack propagation in a two-dimensional macroscopic plate

H Rafii-Tabar, L Hua and M Cross

Nano-Science Simulation Group, Centre for Numerical Modelling and Process Analysis, School of Computing and Mathematical Sciences, University of Greenwich, Woolwich Campus, Wellington Street, London SE18 6PF, UK

Received 4 June 1997, in final form 29 October 1997

Abstract. A novel multi-scale seamless model of brittle-crack propagation is proposed and applied to the simulation of fracture growth in a two-dimensional Ag plate with macroscopic dimensions. The model represents the crack propagation at the macroscopic scale as the drift-diffusion motion of the crack tip alone. The diffusive motion is associated with the crack-tip coordinates in the position space, and reflects the oscillations observed in the crack velocity following its critical value. The model couples the crack dynamics at the macroscales and nanoscales via an intermediate mesoscale continuum. The finite-element method is employed to make the transition from the macroscale to the nanoscale by computing the continuum-based displacements of the atoms at the boundary of an atomic lattice embedded within the plate and surrounding the tip. Molecular dynamics (MD) simulation then drives the crack tip forward, producing the tip critical velocity and its diffusion constant. These are then used in the Ito stochastic calculus to make the reverse transition from the nanoscale back to the macroscale. The MD-level modelling is based on the use of a many-body potential. The model successfully reproduces the crack-velocity oscillations, roughening transitions of the crack surfaces, as well as the macroscopic crack trajectory. The implications for a 3-D modelling are discussed.

1. Introduction

The emergence of an observable fracture on a macroscopic scale is a consequence of crack propagation across several widely different length scales. Traditionally, the continuum-based theories of fracture mechanics [1] have provided the basic computational and modelling tools for studying the fracture processes. These theories provide a variety of energy [2] and force [3, 4] criteria for computing the conditions for further growth of a static crack on the verge of extension. Despite their valuable contributions, a modelling of a fracture process based exclusively on these theories is not, however, capable of accounting for all of the *experimentally* observed characteristics of the crack dynamics or the crack-surface topography. For example, while these theories assume smooth, so-called *mirror-like*, crack surfaces and predict a limiting crack velocity equal to the Rayleigh wave velocity of the material (V_R) [1], recent experimental [5–8] as well as modelling studies [9, 10] clearly suggest that crack surfaces that were originally mirror-like undergo appreciable *mirror-to-mist-to-hackle* roughening transitions, and that crack velocities reach a maximum value of 0.6 V_R. Furthermore, these studies reveal that a *dynamic instability* controls the crack velocity when it exceeds a value of 0.36 V_R, beyond which the crack dynamics changes dramatically, i.e. the mean crack acceleration drops and *violent oscillations* in the velocity set in. *These oscillations lead to the bifurcation of the crack trajectories and the*

0953-8984/98/112375+13$19.50

subsequent emergence of the roughening transitions of the crack surfaces. All of these phenomena remain unexplained within the continuum-based modelling, although there have been attempts [11–13] to provide an insight into the origins of these oscillatory motions. However, these investigations have predicted the onset of these oscillations to be at a velocity of 0.6 V_R, which corresponds to the well-known Yoffe instability [14] and does not explain the value of 0.36 V_R.

Crack behaviour is ultimately determined by the atomic-scale processes occurring within a highly localized and *ultra-fine* volume of the material. This volume forms the nanoscopic *fracture process zone* (FPZ) that surrounds the crack tip. It would, therefore, be reasonable to assume that a *multi-scale* modelling approach that couples the crack propagation across several length and energy scales, e.g. from the centimetre scale down to the nanometre scale, within one unified and *seamless* model would be able to provide deeper insights into the peculiarities of the crack dynamics. In such a model we should be able, in principle, to directly connect the nano-mechanics of the FPZ (for example the sequence of bond ruptures) with the displacement- and stress-field equations of the continuum-based theories and see how macroscopic stresses, applied over macroscopic sample sizes, couple with the local atomistic forces to drive the crack tip forward.

Over the past few years a number of hybrid quasi-continuum approaches to crack propagation have been pursued [15–18] in order to derive a failure criterion from models in which an atomistic core is embedded within a continuum domain. In these models, the energetics of the core is studied via molecular dynamics (MD) simulation, while the continuum is modelled by the finite-element method (FEM). These studies have not, however, been concerned with a multi-scale modelling, although they do constitute the initial attempts in this direction.

We recently performed [19] MD simulations of brittle and ductile fractures in two-dimensional (2-D) triangular lattices of elemental Ag and Ag–Au alloy, using many-body interatomic potentials [20, 21]. In these simulations [19] we correctly predicted the onset of dynamic instability at 0.32 V_R and obtained the associated roughening of the crack surfaces and branching in the Ag. Moreover, the brittle-to-ductile transition in the Ag–Au alloy at elevated temperatures was also obtained. In these simulations [19], we identified the crack tip as the most-stressed atom in the lattice by computing the stress-tensor field over the atomic sites.

In this paper we have substantially extended the above work [19] and have developed a novel multi-scale model of the brittle-crack propagation. In this model, the crack propagation at the macroscopic scale, in real space, is fully parametrized in terms of the *crack-tip data alone* obtained from the nanoscale computations. This is achieved by introducing an intermediate mesoscale continuum to bridge the macroscales and nanoscales. The model is based on a hybrid atomistic-continuum strategy in which the FPZ is represented by a nano-sized atomic lattice located within a continuum with macroscopic dimensions. The novel aspect of the model consists in the way it represents the crack propagation over the macroscopic scale by the drift-diffusion motion of the crack-tip atom alone in the *position* space. In the model, in addition to the *drift* motion of the crack tip, a *diffusive* motion is also introduced so as to accommodate the effect of the crack-*velocity* oscillations, at the atomic level, on the crack *trajectory* (path) at the macroscopic level. The diffusive motion is parametrized by a diffusion constant and a stochastic Wiener process. It will, therefore, generate the roughening transitions at the continuum level. *It should, however, be emphasized that this drift-diffusion motion is not analogous to the usual, thermally driven, diffusion in, for example, a liquid, and should not be interpreted in the same way. In a liquid, a particle diffuses through the system, and at every stage of the process it is the same particle*

that undergoes the diffusive motion, and as the temperature rises the particle diffuses more quickly. Then by considering a set of these particles and averaging over their diffusions, a diffusion constant is obtained. In our model, however, we do not view the crack-tip diffusion within this standard framework. Here, the diffusion does not refer to the motion of the same predefined atom representing the crack tip and moving through the system. Rather, it refers to the stochastic motion of the crack tip, in position space, where the tip is identified with a different most-stressed atom at each stage of the propagation. Furthermore, since we associate the diffusive motion with the crack-tip space coordinates, and not with its velocity, then a rise in the temperature, for example, will only make the crack trajectory more irregular and will not create artificial acceleration or deceleration of the crack. In other words, we represent the sequence of bond rupture events, that characterizes the time evolution of the crack tip in space, by a stochastic drift-diffusion process.

A picture of crack propagation in terms of the motion of the crack-tip atom alone was also recently reported [22], in an MD simulation only, within a non-linear model where the bond-breaking events were separated in time and followed a type of *zigzag* 'ice-skating' sequence, referred to as the Einstein ice-skater model.

In our proposed multi-scale model, the crack propagation involves transitions across three different length and energy scales. These are from the macroscale to the nanoscale, via an intermediate mesoscale continuum, and back to the macroscale again. First, there is the transition from the macroscale to the nanoscale. This essentially involves the computation of the displacements of the FPZ boundary atoms when the macroscopic sample is remotely subjected to applied stresses at its boundaries. From these displacements, the MD-level boundary forces, and hence the MD-level boundary stresses, to drive the crack tip forward within the FPZ are obtained. The calculation of these displacements, as will be discussed, entails the introduction of an intermediate-scale continuum. Next, the nanoscale computations are performed within the FPZ. These will generate the critical crack velocity and the diffusion constant of the crack-tip atom as the bonds break sequentially at the crack tip. Finally, the reverse transition from the nanoscale to the macroscale is concerned with advancing the crack tip to a new position. This is performed by employing the critical crack velocity and diffusion constant in the Ito stochastic differential equation [23] to obtain the crack trajectory.

The following flow chart (figure 1) summarizes the main tasks performed at each of these transitions. We have applied this proposed model to the brittle fracture of a 2-D Ag plate with macroscopic dimensions. The model has a generic structure and can be applied to other metallic and non-metallic elements. Furthermore, as we have indicated at the conclusion of this paper, it can be extended to a 3-D modelling of the fracture phenomena.

2. The transition from the macroscale to the nanoscale

We considered an Ag plate with dimensions of 1 cm along the X-axis and 2 cm along the Y-axis containing an edge crack 0.1 cm in length. In the simulations, the plate was subjected to constant strain rates in the Y-direction. The crack tip was surrounded by a 2-D triangular atomic lattice, representing the FPZ, that was located within an MD cell, and the cell was embedded within the plate. To drive the crack tip forward at the atomic level, we required the forces acting on the boundary atoms of the FPZ. These boundary forces could, in principle, be computed once the displacements of the boundary atoms were known. The FEM can be used to obtain these displacements. However, the straightforward application of the FEM to a multi-length-scale problem such as this entails a severe computational difficulty. This is because the accuracy of an FEM calculation depends crucially on the spatial resolution of its

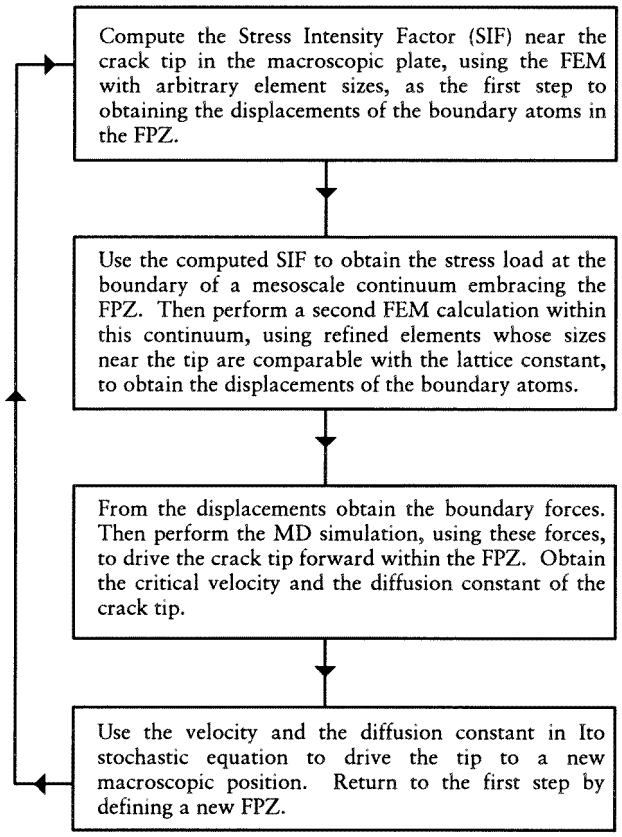

Figure 1. A flow chart summarizing the main tasks.

elements. In our case, this implied that the calculation of displacements at the boundary of the FPZ would have required decomposing the macroscopic plate into elements whose sizes were comparable to the lattice constant of the triangular Ag. This would have made the computation cost prohibitive. To circumvent this problem, we introduced an intermediate mesoscale plate linking the FPZ to the surrounding continuum. The mesoscale continuum had far more refined element sizes than the macroscopic plate, and in the vicinity of the crack tip these sizes were *comparable to the lattice parameter*.

We first employed the FEM, via the software package ANSYS [24], to calculate the stress intensity factor (SIF) for mode I opening (K_I) over the macroscopic plate. In this calculation, we used coarse element sizes. The relation between the SIF and stress load [25]:

$$K_I = \sigma(\pi a)^{1/2}\left(1.12 - 0.23\frac{a}{W} + 10.6\frac{a^2}{W^2} - 21.7\frac{a^3}{W^3} + 30.4\frac{a^4}{W^4}\right) \qquad (1)$$

was then used to obtain the stress load (σ) at the boundary of the mesoscale plate surrounding the FPZ. This plate had dimensions of $4000d \times 1000d$, i.e. 1156 nm $\times$ 289 nm, containing always a crack of the fixed length $100d$; $d = 2.89$ Å is the Ag triangular-lattice parameter. In equation (1), a and W respectively refer to the crack length and the mesoscale plate's width. The underlying assumption in using this equation was that the crack tip was experiencing the same SIF as was produced over the macroscopic plate.

The stress load at the boundary of the mesoscale plate was then used in a second FEM

computation to provide the atomic displacements. Our previous MD simulation [19] had shown that to drive the tip forward, we needed a critical stress load of $\sigma_c = 136.8$ pN/atom.

3. Nanoscale computations within the FPZ

With the computation of the boundary forces, the MD-level simulations were performed to drive the crack tip within the FPZ and obtain the its critical velocity, i.e., the velocity beyond which the dynamic instabilities set in and oscillations are produced, and its diffusion parameter. The lattice chosen consisted of 4970 atoms arranged in 71 rows with 70 atoms per row. The lattice sizes were 20.23 nm $\times$ 17.77 nm, and the MD time-step was $\Delta t = 0.01$ ps. The initial temperature was set at 0 K, but was allowed to evolve freely as the crack propagated. A potential cut-off of $2.25d$ was employed.

The energetics and dynamics of the atoms were obtained from the Sutton–Chen (S–C) potential [20]. The potential parameters are given in [20], but the parameter c in this potential had to be recalculated for the 2-D lattice, and was obtained as $c = 107.7$. The velocity Verlet algorithm [26] was used to integrate the equations of motion.

The S–C potential describes the van der Waals attraction at the long range and combines it with the cohesive interactions at the short range. This potential and its generalization [21] for the fcc binary alloys have been shown to model the mechanical and thermal properties of a range of fcc elemental metals and their alloys quite successfully, and have formed the basis of a series of MD simulations in the past [27, 28].

The crack tip in the MD simulation was identified with the most-stressed atom in the FPZ, and this atom was marked by computing the stresses at atomic sites according to [19, 29] for the S–C potential.

The diffusion constant of the crack-tip atom, at each stage of the propagation, was obtained from the Einstein general model of Brownian dynamics [30]

$$D_0 = \frac{1}{2Nst}\left\langle \sum_{i=1}^{N} |r_i(t) - r_i(0)|^2 \right\rangle \tag{2}$$

where the $\langle\ \rangle$ refers to the averaging over time, the summation refers to the total number of diffusing atoms in the system, s is the dimensionality of the diffusion space; $s = 2$ in the present case, and t is the time. In our simulation, we needed the diffusive motion of a *single* crack-tip atom only. Hence equation (2) reduced to

$$D_0 = \frac{1}{2ts} \sum_{t} |r(t) - r(0)|^2 \tag{3}$$

where $\langle\ \rangle$ is replaced by summation over the (delay) time.

In addition to the diffusion parameter, we needed to calculate the critical velocity. The details of this computation are given elsewhere [19], and the result obtained was $V_m = 605.74$ m s$^{-1} = 0.32\ V_R$. A similar result was also obtained experimentally [5–7] for another material, where it was observed that when an edge crack in polymethylmethacrylate (PMMA) plate started to propagate, the initial speed increased rapidly to about $0.34\ V_R$ and this was then followed by erratic oscillations. A further similar result was also obtained in a large-scale MD simulation [9] using the Lennard-Jones potential. The similarity of all of these results, including ours, obtained for widely different materials, indicates that the value of about $0.32\ V_R$ seems to be a universal critical velocity beyond which the erratic oscillations appear in the crack-velocity profile of the material. We used this value of the V_m in the Ito calculus to advance the crack tip to a new position.

4. The reverse transition to the macroscale

The computation of the critical velocity and the diffusion constant allows the transition from the nanoscale back to the macroscale to occur and hence predicting the macroscopic crack trajectory. This aspect consisted of advancing the crack tip to a new location. Once the tip had advanced to this position, the simulation cycle could be repeated with a new FPZ.

The advancement of the crack tip was based on the Ito stochastic differential equation (see [23])

$$\mathrm{d}X(t) = A[X(t), t]\ \mathrm{d}t + D_0^{1/2}\ \mathrm{d}W(t). \tag{4}$$

This equation describes the stochastic *path*, $X(t)$, of the crack tip, at elevated space and time coordinates, and resembles the position Langevin equation [26]. The term $A[X(t), t]$ is a dynamical variable of the crack tip and is referred to as the *drift* velocity. D_0 is, as before, the diffusion constant and $W(t)$ is a given Gaussian stochastic process, called a Wiener process, with the mean and variance given by

$$\begin{aligned} &\langle \mathrm{d}W(t) \rangle = 0 \\ &\langle \mathrm{d}W_i(t)\ \mathrm{d}W_j(t) \rangle = \delta_{ij}\ \mathrm{d}t. \end{aligned} \tag{5}$$

Equation (4) predicts the increment in position, i.e. $\mathrm{d}X(t) = X(t + \mathrm{d}t) - X(t)$, for a small elevated time interval $\mathrm{d}t$ as a combination of two distinct parts, a smooth (*deterministic*) part represented by $A[X(t), t]\ \mathrm{d}t$, and a stochastic (*random*) part represented by $D_0^{1/2}\ \mathrm{d}W(t)$ and superimposed on the drift part. If we specialize the overall crack-tip motion to an Ornstein–Uhlenbeck-type process [23], then we can identify $A[X(t), t]$ with the *constant* velocity V_m.

Equation (4) is a stochastic differential equation in position space, and associates a stochastic behaviour with the crack-tip space coordinates (trajectory) and not with its velocity. Since the diffusion coefficient appears with the stochastic component of the trajectory equation, then if the temperature of the system were to increase and hence induce a corresponding increase in the value of D_0 (if D_0 were temperature dependent), this would only affect the contribution of the second term in equation (4). It is evident that this would just make the crack trajectory more *irregular*, i.e. one having a more complicated zigzag pattern, and would *not* affect the overall crack drift velocity which is set at the constant critical value of V_m. It should be noted that the rate of crack acceleration is determined by the applied strain. However, as we have shown in our previous simulation [19], different applied strain rates lead to the *same* value of V_m at which the oscillations begin. Furthermore, we should emphasize that equation (4) is *not* concerned with the drift-diffusion motion of a *predefined* atom through the plate, such as is the case in, for example, the diffusion of an interstitial atom through a material. Rather, we could, very schematically, liken the crack-tip diffusion in our case to the diffusion of a vacancy through a plate where the vacancy jumps from one location to the next when *different* atoms recombine with it at different places. It is the *movement* of the crack tip, rather than the movement a fixed atom representing the crack tip, that follows equation (4).

To realize equation (4) in our 2-D simulation, we used the following iterative scheme:

$$\begin{aligned} X(t + \mathrm{d}t) &= X(t) + V_m\ \mathrm{d}t + D_0^{1/2}[\mathrm{d}t]^{1/2} G(t) \\ Y(t + \mathrm{d}t) &= Y(t) + D_0^{1/2}[\mathrm{d}t]^{1/2} G(t) \end{aligned} \tag{6}$$

where $G(t)$ is a standard normal random variable generated according to the procedure given in [26]. The simulation time-step for this part was set at $\mathrm{d}t = 0.01\ \mu$s.

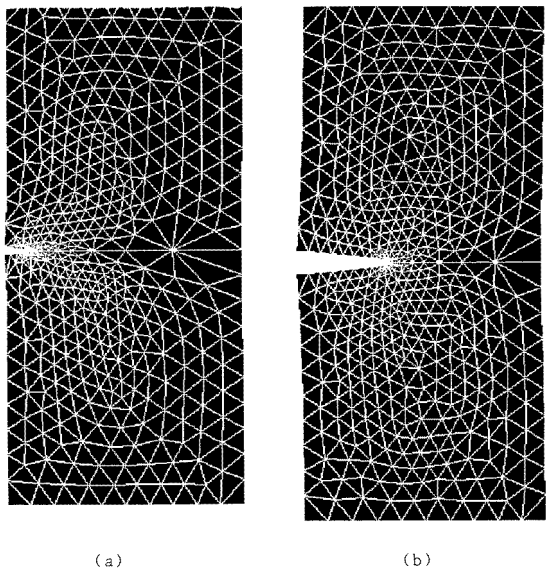

Figure 2. The FEM-based domain decomposition in the macroscopic 1 cm × 2 cm Ag plate containing an initial edge crack of length 0.1 cm along the X-axis: (a) the initial state at the start of the simulation; (b) the state after the crack has propagated for 4.5 μs.

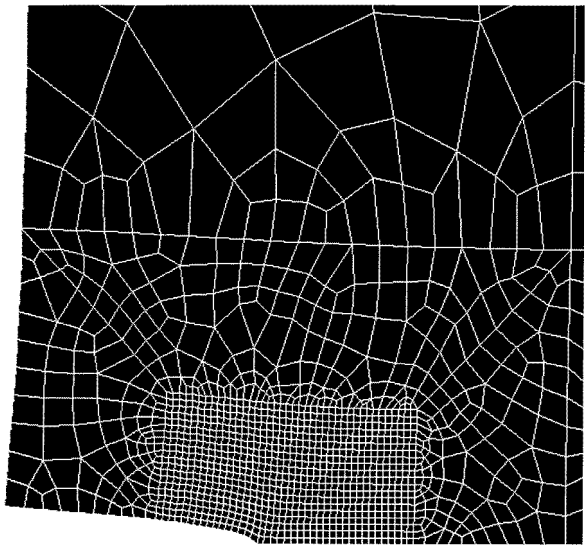

Figure 3. The FEM-based domain decomposition in half of the mesoscale plate surrounding the MD cell. The size of the plate is 1.156 μm × 0.289 μm. The MD cell is located in the region with dense elements whose sizes are comparable with the lattice constant.

5. Results and discussion

Figure 2(a) shows a snapshot of the initial state of the macroscopic Ag plate, containing the initial inserted crack, at the start of the simulation. Figure 2(b) shows the final state

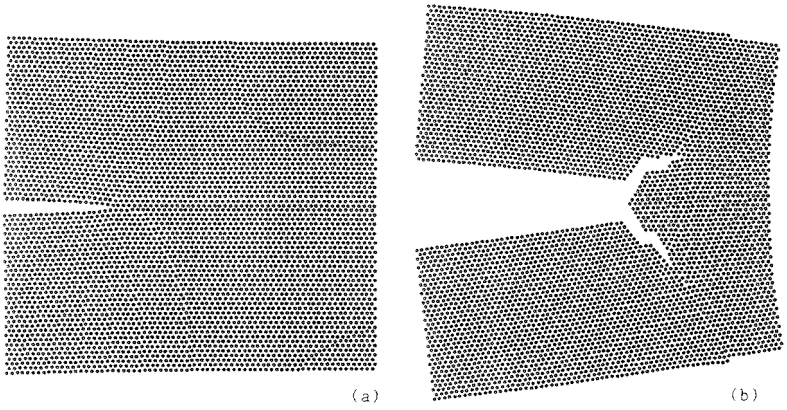

Figure 4. The MD-generated snapshots of the cracked triangular lattice showing (a) the mirror-like initial surfaces; (b) the surfaces after crack bifurcation leading to roughening transitions. The initial temperature was set at 0 K.

of the Ag plate after the crack has propagated forward for 450 dt, i.e. after 4.5 μs. The FEM domain decomposition elements are clearly visible in these figures. Figure 3 shows the domain decomposition, over half of the mesoscale plate, with refined elements. The elements near the crack tip, i.e. the dense area with square-shaped elements, have sizes comparable with the triangular-lattice constant. The MD cell is located within this dense region. The computation of the displacements of the FPZ boundary atoms required element sizes of this order of magnitude. Figure 3 is included to show the intermediate mesoscale continuum that was introduced to bridge between the macroscale and nanoscale FEM calculations. Figure 4 shows two snapshots of the brittle-crack growth in the FPZ. In figure 4(a) the cracked triangular lattice with mirror-like surfaces is shown at the start of the MD simulation, and figure 4(b) shows the state of the lattice at the end of a typical MD simulation where the mirror-like surfaces have clearly undergone roughening transitions. The low simulation temperature did not allow for the appearance of a plastic zone and a brittle-to-ductile transition. Figures 2 to 4 clearly indicate the three different length and energy scales addressed in our simulation.

Starting from the initial coordinates of the crack tip in the X–Y plane at $X = -0.4$ cm and $Y = 1$ cm, three multi-scale simulations were performed for three different constant strain rates of 3.1×10^{-5}, 3.41×10^{-5}, 3.565×10^{-5} applied to the Ag plate boundaries in the Y-direction. In each case the first value of the SIF was calculated and this was then used to obtain the first value of the diffusion constant via the mesoscale and nanoscale computations. The magnitude of the delay time in equation (3) over which the value of the diffusion constant was calculated differed according to the position of the crack tip along its trajectory. Each diffusion constant calculation was performed for a diffusion up to a crack-branching event at the nanoscale. Once the diffusion constant was obtained, the crack tip was moved to a new X–Y position by computing equations (6) for 150 dt, i.e. for 1.5 μs, and then the whole cycle was repeated.

Figure 5(a) shows the variations of K_I, in steps of 150 dt, corresponding to each new set of X–Y coordinates of the crack tip. It is evident from this figure that as the strain rate increased, the values of K_I increased correspondingly, as was to be expected. Moreover, we can see that in all three cases the K_I-values, following their systematic increases, reached maximum values. This was when the crack had advanced to about the midway position in

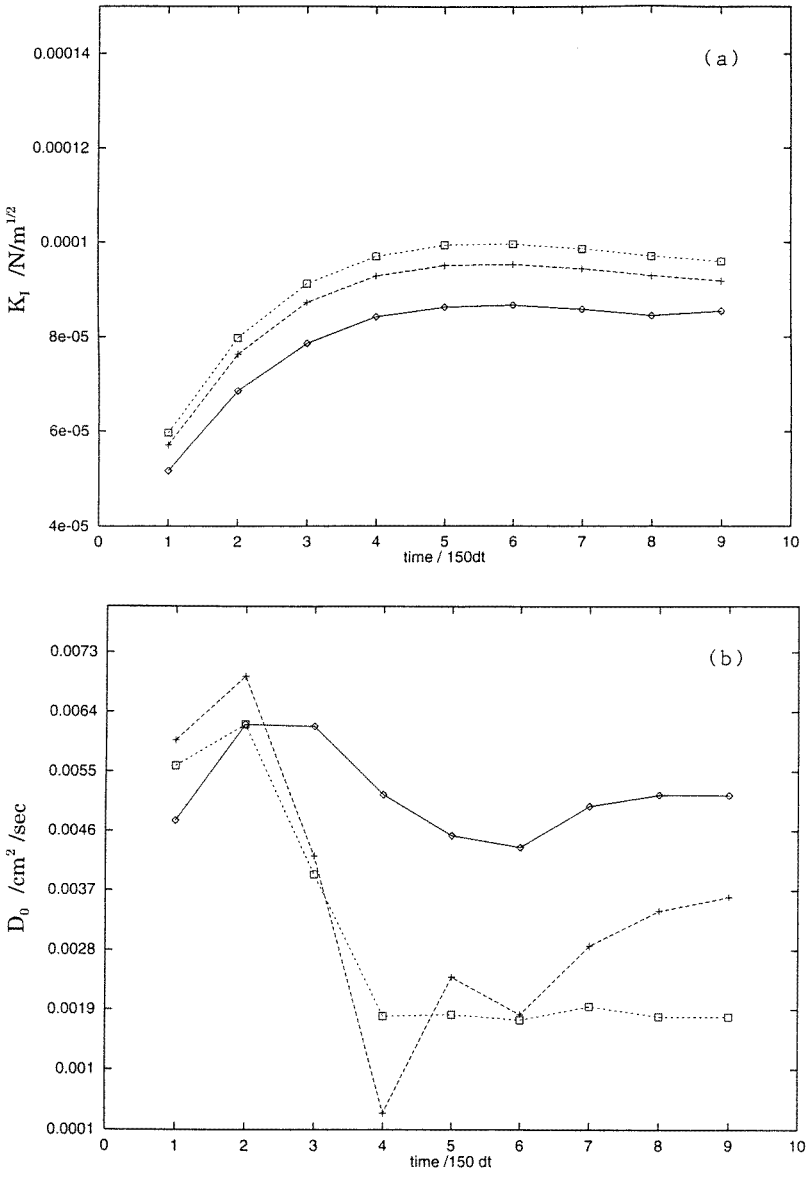

Figure 5. The variations of (a) the stress intensity factor (SIF) at different positions (times) along the crack trajectory in the macroscopic plate for three different strain rates: $\diamond$: 3.1×10^{-5}; $+$: 3.41×10^{-5}; $\square$: 3.5×10^{-5}; and (b) the same for the diffusion constant.

its trajectory. We attribute this behaviour to the finite size of the Ag plate. In a larger plate, the K_I-curves would have continued to increase and the maxima would have been attained at values different to those given here.

Figure 5(b) displays the variations in D_0 corresponding to the variations in K_I. It is interesting to observe that for the higher values of the strain rate, the crack tip diffuses almost uniformly after reaching the half-way position. This implies that a limiting crack diffusion constant, for our sample size, has been reached. This is analogous to the limiting

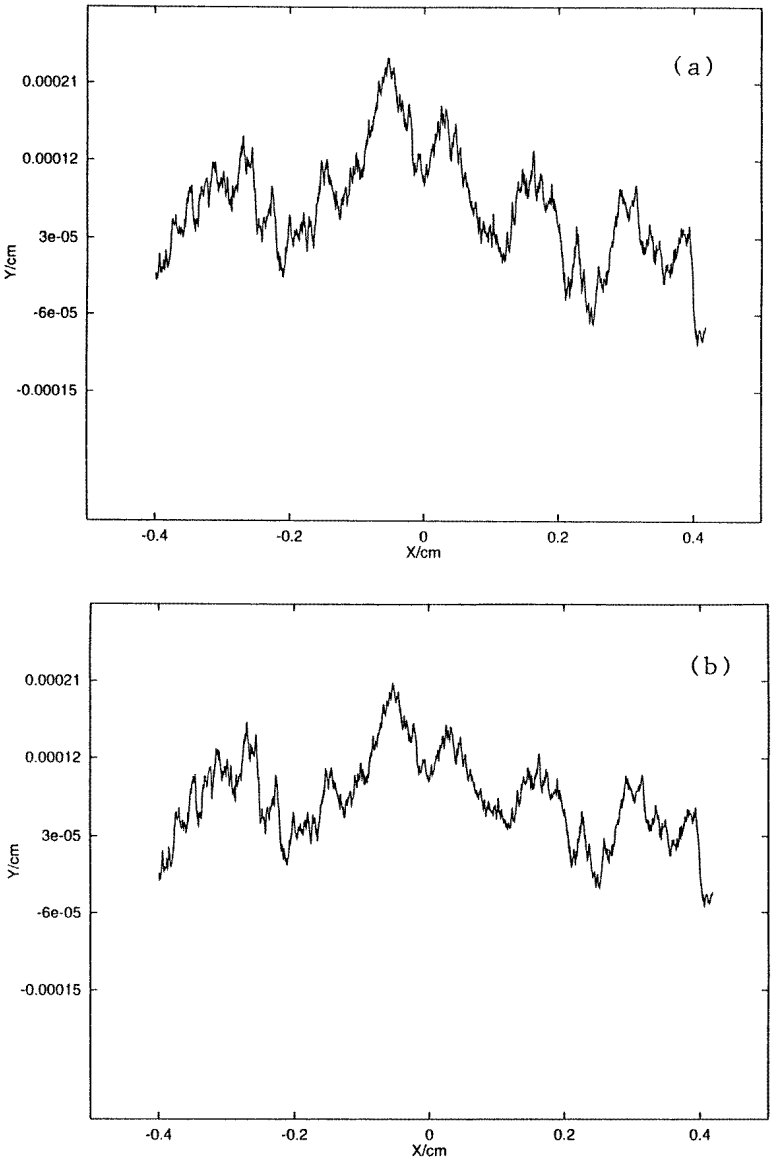

Figure 6. The macroscopic stochastic trajectories of the crack tip for three different strain rates: (a) 3.1×10^{-5}; (b) 3.41×10^{-5}; (c) 3.565×10^{-5}, shown on a submicron segment of the Y-axis. (d) shows the combination of (a), (b) and (c) on a micron segment of the Y-axis.

crack velocity.

Figure 6 shows the stochastic X–Y trajectory of the crack tip, in real space, computed according to equations (6) for three different strain rates. In each of the first three plots in this figure, i.e. (a), (b) and (c), a *submicron* segment of the Y-dimension of the trajectory is depicted so as to reveal fully the details of the stochastic trajectory on this scale. It can clearly be observed from these three plots that the profiles of the *drift* motion of the crack tip are very similar for each case. However, the random component of the trajectory has

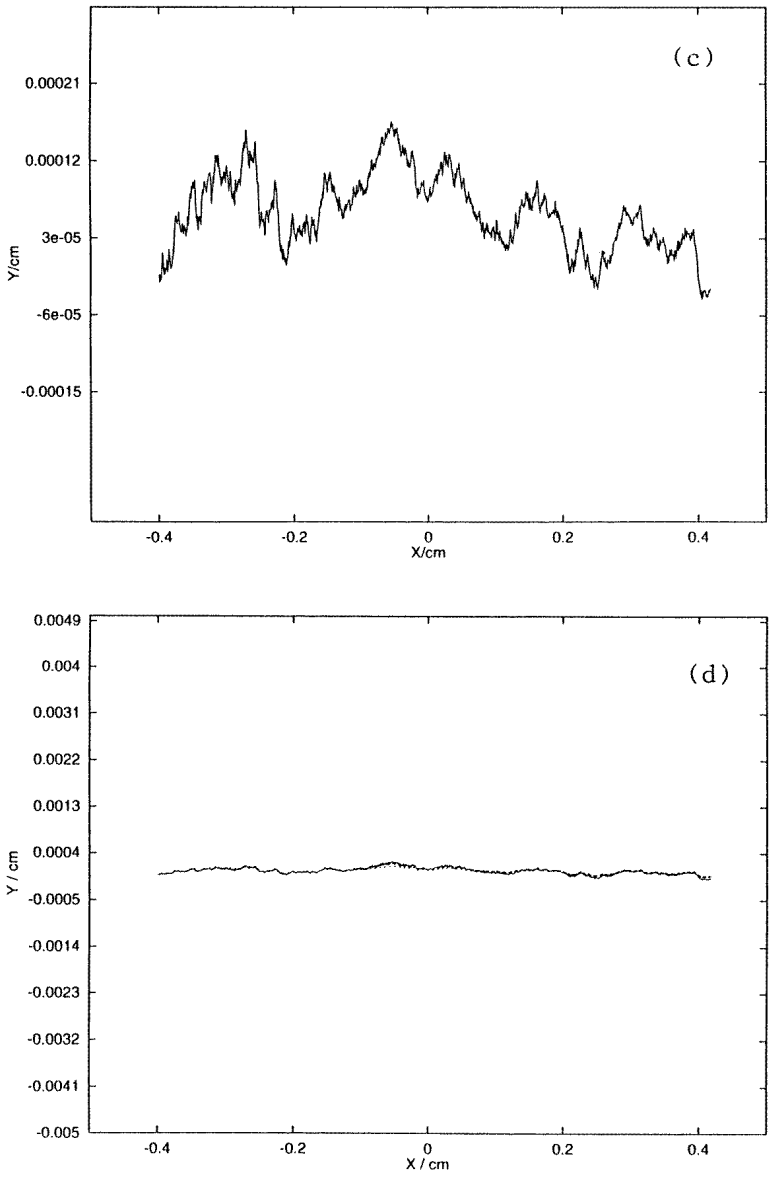

Figure 6. (Continued)

tended to subside with the increasing applied strain. This was in line with the findings shown in figure 5(b) concerning the behaviour of the diffusion constant. In figure 6(d) we have combined the trajectories plotted in (a), (b) and (c), and have given the Y-dimension on a *micron* scale. We can see that, on this scale, the crack trajectories are less hackled and the random fluctuations are to some extent smoothed out. Furthermore, we can identify a micron-size region within which the trajectories are bunched together forming a kind of crack band. This suggests to us that a cleavage crack propagates on a macroscopic scale within a band-like region, i.e. the crack may not have a hair-like feature.

6. Conclusions

In this paper we have provided a generic multi-scale modelling of brittle-crack propagation and applied it to the fracture growth in a 2-D Ag plate with macroscopic dimensions. The model is based on a hybrid strategy and couples the fracture process across three different length and energy scales in which the FEM-based computations of the stress and displacement fields of the continuum mechanics are integrated with the local nanoscale atomistic dynamics. The transition from the macroscale to the nanoscale was achieved via the introduction of an intermediate mesoscale continuum-based calculation of the stress and displacement fields. The nanoscale computations then provided the critical crack velocity and the diffusion parameter of the crack tip. The reverse transition to the macroscale was modelled via the macroscopic Ito calculus in the position space in which the diffusion controls the coordinates of the crack tip. The model has correctly predicted the critical crack velocity and the onset of the roughening transitions of the surfaces associated with the crack-velocity instability. Moreover, due to the multi-scale nature of the model, we have additionally been able to trace the macroscopic crack trajectory in real space in terms of the data generated by the movement of the atomically sharp crack tip. Our nanoscale computations were based on the use of a many-body interatomic potential, and we have found that this potential was reasonably stable, well-behaved, computationally efficient and capable of producing MD results consistent with other MD simulations of the fracture phenomenon.

The model reported here can be further generalized by extending its application to the 3-D simulation of brittle-fracture phenomena. In such an extension, the crack tip will be in the form of a *crack front* composed of a line of atoms. This line can be identified as the set of most-stressed atoms each belonging to a different crystalline plane of the 3-D FPZ. Instead of a single critical velocity and diffusion constant, we then have a set of these values, and a set of Ito equations can then be solved to provide the crack trajectory which now takes the form of a 2-D surface. The 3-D modelling will significantly improve our current description of the fracture behaviour, since a 3-D model will allow for the appearance of plastic deformation, emission of dislocation loops near the crack front [31] and how they affect the further movement of the front, mechanical grooving and the emergence of other topological defects. Above all, it will allow for a realistic comparison to be made with the experimental fracture data on the crack surface topography and fracture toughness. This work is now in progress and will be reported in forthcoming publications.

Acknowledgment

Hua Lu is grateful to the EPSRC for a ROPA-supported post-doctoral fellowship through the Grant GR/K64389

References

[1] Freund L B 1990 *Dynamic Fracture Mechanics* (Cambridge: Cambridge University Press)
[2] Griffith A A 1921 *Phil. Trans. R. Soc.* A **221** 163
[3] Orowan E 1955 *Welding J. (NY) Res. Suppl.* **34** 157s
[4] Irwin G R 1958 *Handbuch der Physik* vol 6 (Berlin: Springer) p 551
[5] Fineberg J, Gross S P, Marder M and Swinney H L 1991 *Phys. Rev. Lett.* **67** 457
Fineberg J, Gross S P, Marder M and Swinney H L 1992 *Phys. Rev.* B **45** 5146
[6] Gross S P, Fineberg J, Maccormick W D and Swinney H L 1993 *Phys. Rev. Lett.* **71** 2417
[7] Sharon E, Gross S P and Fineberg J 1995 *Phys. Rev. Lett.* **74** 5096

[8] Marder M 1997 *New Sci.* **156** (30 August) 32
[9] Abraham F F, Brodbeck D, Rafey R A and Rudge W E 1994 *Phys. Rev. Lett.* **73** 272
[10] Abraham F F 1997 *IEEE Trans. Comput. Sci. Eng.* **4** 66
[11] Langer J S 1993 *Phys. Rev. Lett.* **70** 3592
[12] Langer J S and Nakanishi H 1993 *Phys. Rev.* E **48** 439
[13] Marder M and Liu X 1993 *Phys. Rev. Lett.* **71** 2417
[14] Yoffe E H 1951 *Phil. Mag.* **42** 739
[15] Sinclair J E and Lawn B R 1972 *Proc. R. Soc.* A **329** 83
[16] Mullins M 1984 *Acta Metall.* **32** 381
[17] Kohlhoff P, Gumbsch P and Fischmeister H F 1991 *Phil. Mag.* A **64** 851
[18] Gumbsch P 1995 *J. Mater. Res.* **10** 2897
[19] Hua L, Rafii-Tabar H and Cross M 1997 *Phil. Mag. Lett.* **75** 237
[20] Sutton A P and Chen J 1990 *Phil. Mag. Lett.* **61** 139
[21] Rafii-Tabar H and Sutton A P 1991 *Phil. Mag. Lett.* **63** 217
[22] Holian B L, Blumenfeld R and Gumbsch P 1997 *Phys. Rev. Lett.* **78** 78
[23] Gardiner C W 1985 *Handbook of Stochastic Methods* (Berlin: Springer) pp 93, 106
[24] Kohnke P 1992 *ANSYS User Manual* vol IV (Swanson Analysis System Incorporated)
[25] Hellan K 1984 *Introduction to Fracture Mechanics* (New York: McGraw-Hill) p 244
[26] Allen M P and Tildesley D J 1987 *Computer Simulation of Liquids* (Oxford: Clarendon) p 81
[27] Sutton A P, Pethica J B, Rafii-Tabar H and Nieminen J A 1994 Mechanical properties of metals at nanometre scale *Electron Theory in Alloy Design* ed D G Pettifor and A H Cottrell (London: Institute of Materials) ch 7
[28] Rafii-Tabar H, Kamiyama H and Cross M 1997 *Surf. Sci.* **385** 187
[29] Lynden-Bell R M 1995 *J. Phys.: Condens. Matter* **7** 4603
[30] Hale J M 1992 *Molecular Dynamics Simulation* (New York: Wiley) p 296
[31] Abraham F F 1996 *Forefronts* (the publication of Cornell Theory Centre)